Electronic Preprint for Journal of Information Processing Vol.24 No.4

Regular Paper

Implementing a Rasterization Framework for a Black Hole Spacetime

Yoshiyuki Yamashita[1,a)]

Received: October 26, 2015, Accepted: April 5, 2016

Abstract: The theory of general relativity predicts that the strong gravity of a black hole bends the trajectories of light rays. Calculating their bendings numerically, we can obtain a 3D CG image when the view point is set in the black hole spacetime. The existing researches adopt the ray tracing method for rendering while we adopt the rasterization method in this paper. In order to achieve fast perspective projection in the curved spacetime, we calculate more than thirty million light trajectories on an optimally constructed computational mesh in advance and let a GPU interpolate them when rendering. Furthermore, in order to render the lines and triangular polygons of CG objects accurately, we apply the dynamic subdividing technique (tessellation). Various types of CG programs can be easily written in the same way as in the conventional 3D CG programming with a common graphics API. Utilizing the recent computing power of the GPU, the rendering performance of nearly one million polygons per second is achieved even on a notebook PC.

Keywords: rasterization, black hole, graphics processing unit

1. Introduction

The theory of general relativity that Einstein proposed predicts that the strong gravity of a black hole bends the trajectories of light rays [1], [2]. Calculating their bendings numerically, we can naturally extend the concept of the usual three dimensional computer graphics (3D CG in below) into the black hole's spacetime. Let us call such an extended CG as the *general-relativistic* 3D CG. One of its visual effects is known as a *gravitational lens effect* [3], which has been studied by a number of research papers (e.g., Refs. [4], [5], [6], [7], [8], [9], [10], [11], [12], [13], [14]).

The general-relativistic 3D CG has two kinds of purposes.

One is to contribute to the study of astrophysics, in particular, the study of high energy radiation near around a black hole [4], [6], [7], [13], [14]. In this case the numerical simulation is the main theme to verify with the actually observed data obtained from radio telescopes. Therefore it is almost sufficient to render a simple geometrical shape of a CG object just like a plane, disk, torus, or sphere which represents a model of an accretion disk [3] around the black hole. Due to its simplicity, some of the researches [7], [13] have achieved on-the-fly realtime CG image generation of the gravitational lens effect by utilizing the massive computing power of a recent graphics processing unit (GPU in below).

The other purpose of the general-relativistic 3D CG is to contribute to the field of physics education and/or entertainment that gives an intuitive understanding to high school/junior high school students and amateur scientists who have a particular interest in theory of general relativity [5], [8], [9], [10], [11], [12]. In this case, in contrast to the former case, complex CG objects like space ships, rockets, and so on are preferable for the students and amateurs to feel familiar and intuitive. In the case of conventional 3D CG it is quite common to define the shapes of such space ships and rockets with more than a thousand triangular polygons and render them on GPU by the rasterization framework with common graphics APIs like OpenGL [15] and DirectX [16]. In the general-relativistic 3D CG, in contrast, no research has ever achieved such rasterization based rendering. We challenge it in this paper and fully exploit the graphics processing power of the GPU.

To the author's best knowledge, all the existing research adopt the ray-tracing technique/method but not the rasterization technique/method due to the following two reasons.

(1) The calculation cost of on-the-fly perspective projection in the black hole spacetime is extremely high.

(2) A straight line in the black hole spacetime is not perspectively projected to a straight line but a curved line in general. In the same sense, the three straight lines of a triangular polygon are not projected to straight lines in general.

We solve the problem (1) by constructing a well-formed computational mesh and calculating the light trajectories at all the crossover points on the mesh in advance. The calculation results are loaded to GPU memory and the vertices of CG objects are linearly interpolated by the GPU hardware. Furthermore we solve the problem (2) by applying the dynamic, recursive subdividing technique, often called tessellation, to lines and polygons in the same way as in Refs. [17], [18], [19].

Our system in this paper consists of two stages (see **Fig. 1**). The first half is the *preprocessing stage* to prepare the mesh data. The last half is the actual *rendering stage*, in which the host program is implemented with OpenGL API and the shader programs

[1] Department of Information Science, Saga University, Saga 840–8502, Japan

[a)] yaman@is.saga-u.ac.jp

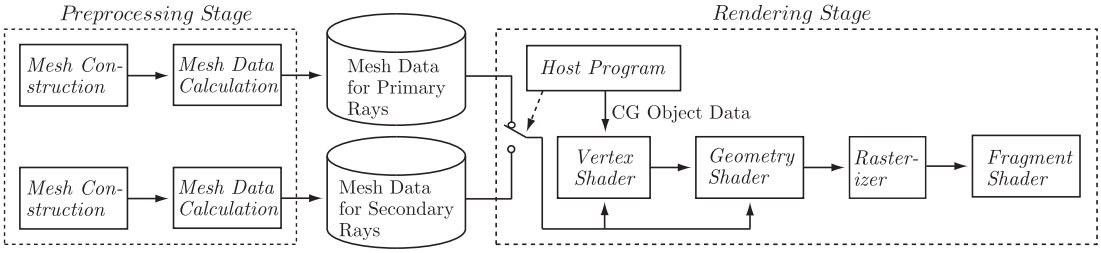

Fig. 1 Overall structure of the CG system consisting of the preprocessing stage and the rendering stage.

on a GPU are written in OpenGL Shading Language [20] (GLSL in below). Because of adopting OpenGL/GLSL framework, we can manage the CG primitives in the same way as in the conventional 3D CG programming. In fact we will show various kinds of CG programs which render point sprites, wireframes, and the 3D modeling data defined by more than a thousand of polygons in the black hole spacetime. The programs can achieve the rendering performances of more than one million polygons per second on the desktop PC, Mac Pro, and nearly one million polygons per second on the notebook PC, MacBook Pro.

The remainder of this paper is organized as follows. In Section 2 we discuss our CG framework (geometry model, rendering method, and color model) that we assume when rendering a CG scene in the black hole spacetime. In Section 3 we explain how to perform the perspective projection by utilizing the trilinear interpolation hardware of a GPU. In Section 4 we actually render the OpenGL primitives: point sprites, lines, and triangular polygons. In particular, lines and polygons are dynamically subdivided to render their distorted appearances accurately. We also discuss the rendering speeds.

2. Framework

In this section we discuss our framework of the general-relativistic 3D CG and the two key problems of the rasterization which we must solve.

2.1 Geometry Model

Figure 2 illustrates the geometrical model in this paper, where the gray disk with white letters "BH" in the figure represents the black hole. A light ray (each of the solid and dashed arrows in the figure) is assumed to be emitted from a point P on a polygon surface of a self illuminating CG object, or emitted from a certain light source and then reflected at the point P. Such a ray passes near a black hole, then proceeds through a pixel point S on a perspective screen, and then finally reaches a view point V. Because the ray bends by the strong gravity of the black hole, there can be more than one such ray that goes through both P and V. In Fig. 2 there are the two rays of solid and dashed arrows that go through the points S and S', respectively. Note that, if the light source exists, the ray trajectory from the light source to P (the gray bold arrow in Fig. 2) also bends near the black hole. However, in order to reduce the calculation cost, we simply assume that the line segment of such a ray from the light source to P does not bend and that the polygon is rendered according to Phong's shading model [21] with an ideal parallel light source at infinity.

We fix the black hole at the origin of the world coordinate system (or global coordinate system). In this sense, we implicitly identify the world coordinate system with the black hole spacetime coordinate. The type of the black hole we discuss here is the simplest, spherically symmetric one, called *Schwarzschild black hole*, which is defined by the following Riemann metric [1], [2]

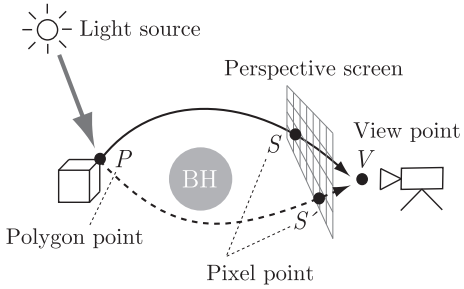

Fig. 2 Geometrical framework among a polygon, a perspective screen, and a view point.

$$ds^2 = \left(1 - \frac{a}{r}\right)dt^2 - \left(1 - \frac{a}{r}\right)^{-1} dr^2 - r^2\left(d\theta^2 + \sin\theta d\phi^2\right) \quad (1)$$

where the triplet (r, ϕ, θ) expresses the polar space-like coordinates and t the time-like coordinate. The constant a, called a *gravitational radius*, defines the radial boundary between the inside ($r < a$) and outside ($r > a$) of the black hole, where we consider only the outside for the view point and polygon points. The trajectory of every light ray is defined by a set of second-order, nonlinear, ordinary differential equations, called a *geodesic equations*, derived from the Riemann metric according to the theory of general relativity (see the details in Ref. [1]). In our case of Eq. (1), because of the symmetricity of the black hole, we can omit the coordinate θ by fixing $\theta = \pi/2$ so that, without the loss of generality, the ray trajectory can be defined by the following set of three equations,

$$\begin{aligned} \ddot{t} &= -\frac{a}{r^2}\left(1 - \frac{a}{r}\right)^{-1} \dot{t}\dot{r} \\ \ddot{r} &= -\frac{1}{2}\left(1 - \frac{a}{r}\right)\left(\frac{a\dot{t}^2}{r^2} - \frac{a\dot{r}^2}{(r-a)^2} - 2r\dot{\phi}^2\right) \\ \ddot{\phi} &= -\frac{2\dot{r}\dot{\phi}}{r} \end{aligned} \quad (2)$$

where the dot $\dot{}$ and the double dot $\ddot{}$ mean the first and second order derivation operators $d/d\lambda$ and $d^2/d\lambda^2$, respectively, with an arbitrary parameter λ. There are two kinds of methods available to solve Eq. (2). One method is to use the fourth-order Runge-Kutta integration as many existing research do [4], [7], [8], [9], [10]. The other method is to use the analytic solution [13].

2.2 Problems of Rasterization

To the author's best knowledge, all research up to now adopt

the ray tracing method [*1], which traces the light ray trajectory in Fig. 2 back in time. Mathematically speaking, the ray tracing method must solve the *initial value problem* (IVP in below) of Eq. (2), that is, given an arbitrary view point V and an arbitrary pixel point S (or S') on the perspective screen, we first calculate the initial point and initial direction of the light ray, then trace the ray trajectory according to Eq. (2), and obtain the point [*2] P on a certain polygon surface if there exists such a surface that the ray hits on. This calculation cost is expensive but, with the computing power of a recent GPU, several research effort/paper [7], [13] have accomplished solving the IVP on the fly and generating CG images in realtime. However they treat a considerably simple geometrical shape of a CG object like a plane or a disk. The rendering programs are specialized to their specific CG objects. When challenging to render more complicated objects that may be defined by more than a thousand of polygons, it seems still hard to render them in realtime by the ray tracing method.

In contrast to the existing researches, we adopt the rasterization in this paper. One of the benefits of the rasterization is that, because it is the fundamental framework for all commercial GPU, we expect that we can fully exploit the hardware performance of the GPU. The other is that we can write the general-relativistic 3D CG programs in the same manner as we write usual 3D CG programs with common graphics APIs. In fact, various CG examples are given in Section 4. On the other hand, we must herein focus on two key problems, which are the main reasons why the existing researches do not adopt the rasterization method.

One problem is that we must solve the *boundary value problem* (BVP in below) of Eq. (2) to implement the rasterization in the black hole spacetime. That is, given an arbitrary view point V and an arbitrary polygon point (vertex) P, we must calculate the light ray that goes through both V and P and obtain the pixel point S (or S') on the perspective screen that the ray trajectory crosses. In general, solving the BVP is more expensive than solving the corresponding IVP. A standard method of solving the BVP is to use the bisection algorithm (or its improved algorithm) of iteratively solving the IVP, and therefore it is unacceptable for fast on-the-fly rendering. Another method is to use the analytic solution of Eq. (2). However, the calculation cost does not decrease drastically because the solution contains a couple of Jacobi elliptic functions [13].

For these reasons, we propose another method of utilizing the hardware linear interpolation unit of a GPU, though the idea is not new at all. Our system consists of the preprocessing stage and the rendering stage, as illustrated in Fig. 1. In the preprocessing stage we first construct a computational mesh, then solve the BVP for every mesh point, and store the calculation results (a set of BVP solutions) into a hard disk. Next, in the rendering stage, for given arbitrary V and P, the solution is linearly interpolated from the pre-calculated solutions loaded from the hard disk. Now arises the question whether the interpolation error can be sufficiently small or not. The answer is yes when we prepare enough number of solutions on a deliberately constructed mesh. The rendering cost is expected to be particularly smaller than those of the above two on-the-fly methods because we do not solve the BVP on the fly and use the GPU hardware effectively. The key point is how to construct an optimal structure of computational mesh. We will discuss the details of mesh construction in Section 3.

The other technical problem of the rasterization is that a straight line in the curved spacetime is perspectively projected to a curved line but not a straight line in general due to light ray bending. Thus we cannot use the common rasterization method. To solve this problem, we apply the subdividing technique that divides a given line into two or more shorter lines recursively and then rasterizes the lines. If the divided lines are shorter enough such as the approximation errors are on the sub-pixel scale, the human eye cannot recognize the errors. The same technique is also applicable to a triangular polygon. In this paper we implement this technique on the geometry shader of a GPU (see Fig. 1). The details are explained in Section 4.

Here we put one more assumption that any polygon point P stands at rest in the black hole spacetime or moves slowly enough, because it is too complex to trace P when P moves with semi-light speed. In contrast, the view point can move at any speed if the speed is not beyond the light speed. In this case it is enough to insert the Lorentz transformation (see Ref. [14] from the view point of the 3D CG on special relativity) after the usual viewing transformation and before perspective projection over the whole sequence of 3D CG coordinate transformations.

2.3 Color Model

One of the visual effects necessary for the relativistic 3D CG is the red/blue-shift of light frequency due to gravitational potential and/or the Doppler shift of light. In order to implement this effect simply in a CG program, we assume that the rendering color of every CG object is approximately represented with the color temperature of an ideal black body radiation. Because it is known that the ratio of the light frequency change is equivalent to that of the temperature change in the case of black body radiation [22], given the original temperature T of the CG object and the ratio f of the light frequency change (see Section 3.4), the temperature T' that the view point observes is simply calculated as $T' = fT$, and further translated into the RGB color (r', g', b') on the perspective screen.

3. Fast Perspective Projection by Trilinear Interpolation

In this section we first clarify our requirements for the perspective projection in the black hole spacetime. Next, we optimize the structure of the computational mesh for interpolating the perspective projection.

3.1 Requirements for Perspective Projection

Due to the spherical symmetricity of the black hole, every light ray we discuss here travels along the plane that contains the view point V, the center O of the black hole, and the polygon point P. Thus it is enough to treat the perspective projection only on this plane.

[*1] Precisely speaking, the method we mention here is the ray casting method which includes no multiple trace of reflective and refractive rays.

[*2] Note that Fig. 2 may be misleading in the case of ray tracing because P is usually an inner point of a polygon surface but not a polygon vertex.

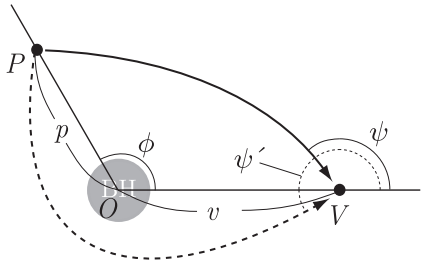

Fig. 3 Simplified geometry model for the primary and secondary rays.

Now let us consider a light ray such that starts from P, goes around the black hole less than 180° of angle, and then reaches V. We categorize such a ray as the *primary light ray*, whose trajectory is illustrated as the solid line in **Fig. 3**. In this case, the incident angle ψ of the light ray to the view point V can be uniquely determined by the following three parameters:

(1) the radial coordinate value [*3] p ($\in [a+\epsilon, R_{\max}]$) at P,
(2) the angle ϕ ($\in [0, \pi]$) enclosed by P, O, and V, and
(3) the radial coordinate value v ($\in [a+\epsilon, R_{\max}]$) at V,

where $[a+\epsilon, R_{\max}]$ specifies the range at which we can arrange the view point and polygon vertices. We set $\epsilon = 0.01a$ and $R_{\max} = 500a$ here. Once we obtain the angle ψ, the projected point S on the perspective screen can be easily geometrically calculated. Let us categorize another type of ray such that starts from P, goes around the black hole more than or equal to 180° and less than 360° of angle, and reaches V, as the *secondary light ray*, whose trajectory is illustrated as the dashed line in Fig. 3. Its incident angle ψ' can also be uniquely determined by the given triplet (p, ϕ, v). Theoretically, we can also consider other types of rays that go around the black hole more than 360° of angle. We however discard them because the incident angles of such rays are contained within a quite narrow range and therefore the images of CG objects rendered with this kind of light rays are negligibly small.

As a consequent, if the points P, O, and V are given,

(1) we first determine the plane that contains all the three points,
(2) calculate the three parameters p, ϕ, and v,
(3) obtain the incident angles ψ and ψ' from the triplet (p, ϕ, v), and
(4) calculate the points S and S' on the perspective screen.

Because ψ and ψ' obtained from (p, ϕ, v) can be recognized as the three argument functions $\psi(p, \phi, v)$ and $\psi'(p, \phi, v)$, respectively, we can expect to use the hardware trilinear interpolation unit on GPU with 3D textures to obtain the function values. Therefore this technique of utilizing the trilinear interpolation is not applicable when more than three parameters are required to calculate ψ (or ψ'). Hence we note that our technique in this section is restricted for the spherically symmetric black hole and not applicable for black holes having more degrees of freedom. For example, the research paper [7] roughly estimates the potential of the interpolation for fast ray tracing in the case of the axi-symmetric black hole [2] and concludes that it is ineffective.

[*3] Note that this is not the *physical* distance from O to P because a physical distance between inside and outside of the black hole cannot be defined in Eq. (1).

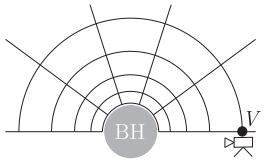

Fig. 4 Black-hole-centric mesh structure.

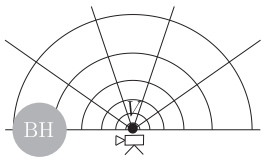

Fig. 5 View-point-centric mesh structure.

3.2 Mesh Structures for Perspective Projection

A 3D texture can be used not only for representing volumetric data in a CG scene but also for representing a function of three input parameters if the function becomes smoother as the interpolation error becomes smaller. Although the default mesh structure of the 3D texture is a cube of size 1 (= $[0, 1]^3$), we can change the structure by apply coordinate transformations so as to decrease the interpolation error. The aim of this section is to obtain an optimal mesh structure suitable for the functions $\psi(p, \phi, v)$ and $\psi'(p, \phi, v)$ discussed in the previous subsection.

Before proceeding to searching for the optimal mesh structure, let us estimate the permissible upper limit of the interpolation error $\Delta\psi$ of the incident angle. Suppose that the horizontal pixel resolution of the CG images is 2,000 and that the horizontal angle of view of the virtual camera is 40° [*4]. Thus, letting Δp be the error of the pixel position on a CG image, the error of the angle is derived as follows.

$$\Delta\psi = \frac{40^\circ}{2{,}000}\Delta p = 0.02^\circ \Delta p$$

If we give the condition $\Delta p < 1$, that is, the error is on the sub-pixel scale, it is implied that $\Delta\psi < 0.02^\circ$. This is the maximum permissible error of the incident angle.

The simplest mesh structure is identified with the structure of the triplet (p, ϕ, v) itself, of which the two dimensional substructure (p, ϕ) is regarded as the black-hole-centric mesh structure illustrated in **Fig. 4**. This structure however is not acceptable for the primary rays because the interpolation errors around the view point are beyond the above permissible upper limit no matter how many mesh points are added to the mesh, that is, the mesh boundary does not match with the view point. In the similar reason, the view-point-centric mesh structure illustrated in **Fig. 5** is also unacceptable due to the errors near around the black hole.

To resolve these problems, we introduce a new mesh structure $(s, t, u) \in [0, 1]^3$ that matches with both the boundaries of the view point and the black hole. **Figure 6** illustrates its sub-mesh (s, t), which consists of two kinds of circular arcs. One is the arc whose circular center is located on the line along the center of the black hole and the view point (see the arcs with parameter $s = 0.1, 0.2, \ldots, 0.9$ in Fig. 6). The other is the arc that passes through both the center of the black hole and the view point (see the arcs with parameter $t = 0.1, 0.2, \ldots, 0.9$ in Fig. 6). Mesh points are the crossover points of these two kinds of arcs. The calculation cost of the coordinate transformation $(p, \phi, v) \mapsto (s, t, u)$ is not very large because it requires at most 40 arithmetic operations, three square-root operations, and one arctangent operation (the details are omitted due to the limited paper space). Next, in

[*4] The value 40° is the horizontal angle of view of a standard 50 mm lens on a 35 mm film camera. The permissible upper limit $\Delta\psi$ of the error becomes larger (more relaxed) if we use wider angle of view.

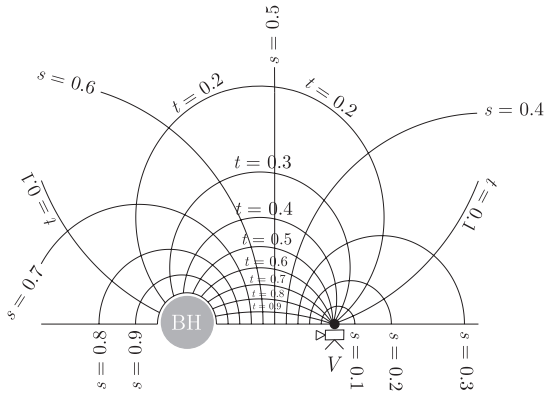

Fig. 6 Mesh structure (s,t) matched with the black hole boundary and the view point boundary.

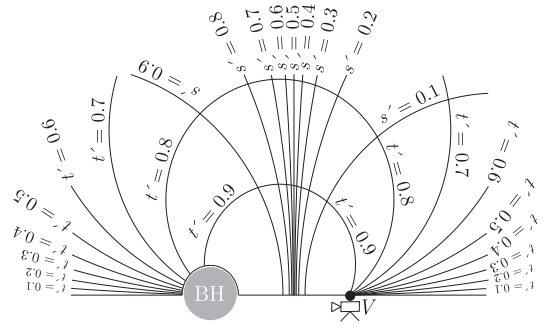

Fig. 7 The optimal mesh structure (s',t') transformed from Fig. 6.

order to accommodate further smaller errors, one more coordinate transformation from (s,t,u) to a new mesh $(s',t',u') \in [0,1]^3$ is introduced. **Figure 7** illustrates such an example of the optimal sub-mesh (s',t') exhaustively obtained by the method explained in the next subsection. As a result, we can construct the optimized mesh for the primary rays by the two successive coordinate transformations: $(p,\phi,v) \mapsto (s,t,u) \mapsto (s',t',u')$.

Different from the primary light ray, we can use the black-hole-centric mesh (p,ϕ,v) for the secondary ray (see Fig. 4) and there is no need for concern about the boundary matching with the view point since the secondary ray goes around the black hole at least 180° so that any polygon point is regarded as sufficiently far from the view point even if they are geometrically close in the coordinate system. In order to normalize the mesh domain and accommodate smaller errors, the mesh (p,ϕ,v) is transformed to a new mesh coordinate $(s'',t'',u'') \in [0,1]^3$.

3.3 Exhaustive Search of the Optimal Mesh

According to OpenGL, a 3D texture has the size of $2^i \times 2^j \times 2^k$ $(i,j,k > 1)$ and the corresponding memory size is its multiple by 16. For example, the setting $i = j = 8$ and $k = 7$ requires 128 megabytes of memory on GPU.

Given a memory size M, the author has exhaustively searched the optimal mesh structure (such as Fig. 7) for the primary rays as follows.

(1) Initialize the sizes (triplet of integers) (i,j,k) of the 3D texture such as $16 \times 2^{i+j+k} = M$.
(2) Initialize the shape of the mapping $(s,t,u) \mapsto (s',t',u')$ in some way.
(3) Calculate ψ for each of 2^{i+j+k} crossover points on the mesh (s',t',u') by solving the BVP [*5] of Eq. (2).
(4) Check the error $\Delta\psi = |\psi - \tilde{\psi}|$ between the true angle ψ and the linearly interpolated angle $\tilde{\psi}$ at each of four million test points chosen different from the crossover points on the mesh, and summarize the maximum error $\Delta\psi_{\max}$, the average error $\overline{\Delta\psi}$, and the average plus the three standard deviation $\overline{\Delta\psi} + 3\sigma$.
(5) Modify the shape of the mapping $(s,t,u) \mapsto (s',t',u')$ in some way (with the idea of the so-called hill-climbing but almost randomly) and goto to Step (3).
(6) Determine the optimal mesh such that it gives the minimum $\overline{\Delta\psi} + 3\sigma$ for the texture sizes (i,j,k).
(7) Modify the texture sizes (i,j,k) under the restriction $16 \times 2^{i+j+k} = M$ and goto to Step (2).
(8) Determine the couple of the texture sizes (i,j,k) and the optimal mesh such that it gives the minimum $\overline{\Delta\psi} + 3\sigma$ for the given memory size M.

In the same way, the optimal mesh for the secondary rays is determined.

Table 1 Linear interpolation error of the incident angle ψ for primary light rays in terms of required memory size of mesh data.

Memory (MB)	$\Delta\psi_{\max}$	$\overline{\Delta\psi}$	$\overline{\Delta\psi} + 3\sigma$
64	0.609	0.008	0.059
128	4.014	0.007	0.043
256	0.242	0.005	0.039
512	0.226	0.002	0.018

Table 1 shows the experimental results of the interpolation errors for the primary rays in terms of the GPU memory usage. We see that $\overline{\Delta\psi} + 3\sigma$ is under the maximum permissible error 0.02° when the texture memory size is 512 megabytes [*6]. Thus we can statistically estimate that 99.7% [*7] of the interpolation errors are on the sub-pixel scale. On the other hand, $\Delta\psi_{\max}$ indicates that the errors are far bigger than the permissible error at some test points [*8]. However, it does not seriously affect our research because other kinds of experiments we omit to give here show that such test points exist near at $v \approx R_{\max}$. Hence we can prevent them by putting the view point not far from the black hole. If we intend to put the view point far from the black hole, that is, we render super-telephoto images, we should construct a new mesh structure optimized for the super-telephoto condition, in which case we expect that we can use the black-hole-centric mesh in Fig. 4 instead of the complex mesh in Fig. 6 because no polygon point overlaps with the view point.

Table 2 shows the results for the secondary rays; the errors in this table are small enough even if we use a 3D texture of 16 megabytes.

It took about 116 hours and 114 hours to search for the optimal

[*5] The author applied the bisection method of iteratively solving the corresponding IVP.
[*6] In this case, $i = j = 9$ and $k = 7$. The number of mesh points is $2^{9+9+7} = 2^{25}$, which is about thirty million.
[*7] The actual ratio the author counted from the experimental results is 99.5%.
[*8] The maximum error 4.014 in the case of 128 megabytes in Table 1 means that the searching procedure falls into the local minimum in this case because we focus on only the value of $\overline{\Delta\psi} + 3\sigma$. As a matter of fact the second best solution gives $\Delta\psi_{\max} = 0.609$, $\overline{\Delta\psi} = 0.006$, and $\overline{\Delta\psi} + 3\sigma = 0.056$.

Table 2 Linear interpolation error of the incident angle ψ' for secondary light rays in terms of required memory size of mesh data

Memory (MB)	$\Delta\psi'_{\max}$	$\overline{\Delta\psi'}$	$\overline{\Delta\psi'} + 3\sigma'$
4	0.044	0.005	0.026
8	0.044	0.003	0.020
16	0.041	0.003	0.018
32	0.029	0.002	0.012

mesh structures and calculate the mesh data for the primary and secondary rays, respectively, by using a Mac Pro (Mid. 2012, 12 cores of Intel Xeon 2.4 GHz) in a MPI-based parallel computing environment [23].

3.4 Additional Data Set

In addition to calculate ψ and ψ', the following values are necessary to implement realistic shading for polygons:

(1) the emission angle γ of the light ray at the polygon point P, which is used for the calculations of diffusion and reflection of Phong's shading model [21],

(2) the length $L = \int_P^V d\lambda$ of the ray trajectory from P to V (recall Eq. (2)), which is used for the depth buffer hidden surface algorithm, and

(3) the ratio $f = e'/e$ of the light ray's energy e' at V to the same ray's energy e at P, which is used for the calculation of red/blue-shift of the light ray frequency (see Section 2.3).

As a consequence, we must prepare two kinds of mesh data $(s', t', u') \mapsto (\psi, \gamma, L, f)$ and $(s'', t'', u'') \mapsto (\psi', \gamma, L, f)$ in the preprocessing stage.

Encapsulating the difference of the above two mesh data for the primary and secondary rays, we can write only one set of programs for the vertex, geometry, and fragment shaders common to both kinds of light rays. When executing the set of the shader programs, we first execute them with the mesh data for the primary rays and next execute them with that for the secondary rays by switching the data (see the switching circuit controlled by the host program in Fig. 1).

4. Rendering OpenGL Primitives

In this section we explain the rendering techniques of OpenGL primitives: point sprites, lines, and triangular polygons in the black hole spacetime.

For help in understanding of each CG image example in this section, four scene conditions: the horizontal angle of view, the radial coordinate value v at the view point, the radial coordinate value p_o at the center position of each 3D object, and the size (or length, width) s_o of the object, are noted in the caption of each figure, where v, p_o, and s_o are expressed as multiples of the gravitational radius a introduced in Eq. (1). The view point and objects are assumed to be at rest or move slowly near the black hole. Note that such a CG image is not yet intended to strictly render a physically realistic situation but is mainly used to check whether our rendering algorithm works as expected or not. More realistic rendering is one of our future works (see Section 5).

4.1 Rendering Point Sprites

Point sprites can be rendered in the same manner as in the usual OpenGL/GLSL manner [21]. The CG image in **Fig. 8** shows such an example that renders a star field having tens of thousands of stars [*9] on the celestial sphere. The view point exists near the black hole and watches the direction of the black hole. The black blank circular area at the center of Fig. 8 is considered to be the visual appearance of the black hole because no light ray from the black hole can reach the view point. Big, bright stars apart from the black hole are rendered with the primary rays, while small, dark ones near around the black hole are rendered with the secondary rays.

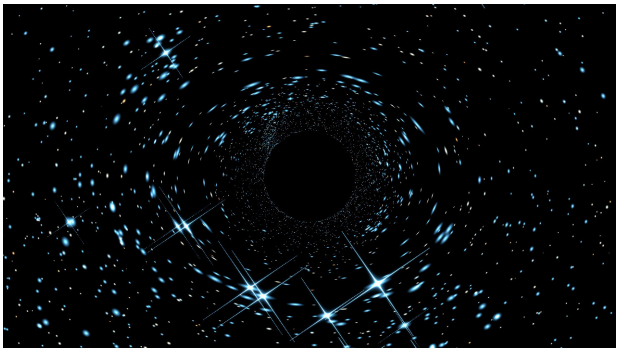

Fig. 8 CG image of a star field around a black hole. Stars are implemented by point sprites. The horizontal angle of view is 60°. The view point is at $v = 30a$ and the radius s_o of celestial sphere is $200a$.

Note that the visual solid angle $d\Omega'$ of a star in the black hole spacetime differs from the corresponding solid angle $d\Omega$ in the flat spacetime due to the bending of light rays, and that the star becomes brighter than usual if $d\Omega' > d\Omega$ and vice versa. Hence we must prepare the ratio $d\Omega'/d\Omega$ at the same time as we prepare the quadruplet (ψ, γ, L, f) in the preprocessing stage (recall Section 3.4). Various shapes of stars including the cross shapes of brighter stars are implemented in the same way as in the book [21].

4.2 Rendering Lines

Lines can also be used in our rendering system. The difference from the usual OpenGL usage is that a straight line near around the black hole is not projected to a straight line on the perspective screen in general due to the light ray bending.

Figure 9 (a) illustrates an example of inaccurate projection of a straight line. Suppose that the primary light rays perspectively project the two end points P_1 and P_2 of the line to the points S_1 and S_2 on the perspective screen, respectively. The usual rasterizing algorithm draws the straight line S_1S_2 while the accurately projected shape of the line could be the dashed, curved one in the figure. Similarly, the secondary light rays project P_1 and P_2 to S'_1 and S'_2, respectively, and the straight line $S'_1S'_2$ is drawn, which is also inaccurate in general.

In order to rasterize the accurate shape, we apply a recursive subdivision method [17] to line rendering. Figure 9 (b) illustrates the first level subdivision; the midpoint P_m between P_1 and P_2 is projected to the point S_m by a primary ray, and the two straight lines S_1S_m and S_mS_2 are drawn. Similarly, the same P_m is projected to S'_m by a secondary ray, and the two straight lines $S'_1S'_m$

[*9] To make natural, realistic CG image, the positions and colors (color temperatures precisely) of the stars are obtained from Yale Bright Star Catalog [24].

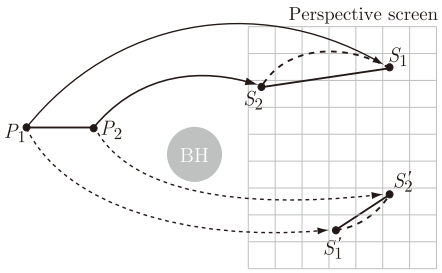

(a) No line subdivision

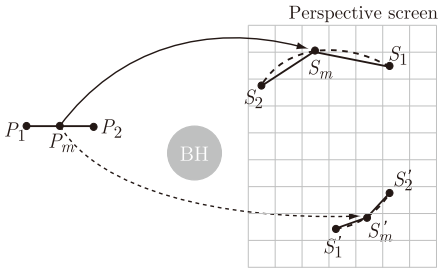

(b) The first level line subdivision for primary and secondary light rays

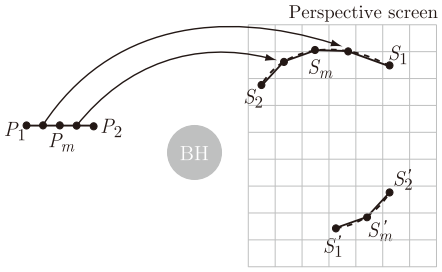

(c) The second level line subdivision for primary light rays

Fig. 9 Line subdividing procedure in a black hole spacetime.

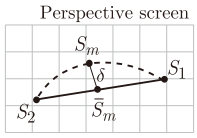

Fig. 10 Terminating condition for recursive line subdivision.

and $S'_m S'_2$ are drawn. Figure 9 (b) shows a better approximation than Fig. 9 (a). The condition for terminating the recursive subdivision is whether the pixel distance δ (see **Fig. 10**) between the projected point S_m and the mid point S'_m between the projected points S_1 and S_2 is smaller than a certain threshold Δ, that is, $\delta < \Delta$. We set $\Delta = 1$ in our implementation so that the approximation error of the subdivision can hardly be recognized by human eyes. Figure 9 (c) illustrates the case that the subdividing does not terminate for the primary rays but terminates for the secondary rays. The author implemented this dynamic, recursive line subdividing algorithm on the geometry shader (see Fig. 1) of a GPU. The recursion must also be terminated if the number of lines recursively generated is beyond the hardware upper limit of the geometry shader's output buffer.

For example, **Fig. 11** is the wireframe image of the Utah teapot of astronomical size; though the situation is quite unusual. The ring shape of the distorted image is called the *Einstein ring* [2]. It is known that the sun in our solar system has a gravitational radius of approximately 3.0 km if the sun became a black hole [2].

Fig. 11 Wireframe image of Utah teapot near a black hole. The horizontal angle of view is 50°. The view point is at $v = 10a$, the center of the teapot is at $p_o = 5a$, and its size s_o is $2a$.

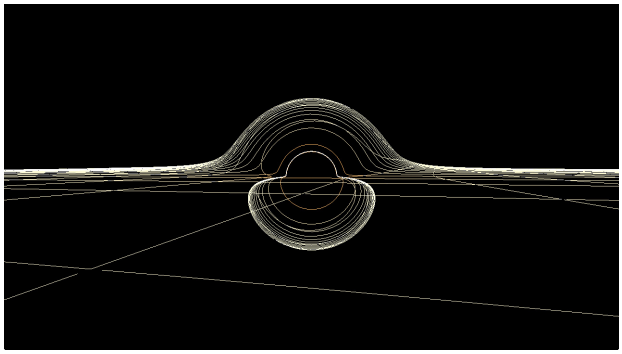

Fig. 12 CG image of the *x*-*y* mesh lines near around a black hole. The horizontal angle of view is 60° and the view point is at $v = 30a$.

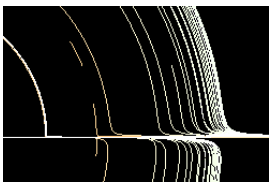

Fig. 13 An enlarged part of a CG image in the case that the geometry shader's output buffer is overflown.

Under this assumption, the view point in Fig. 11 is at $v = 30.0$ km, the center of the teapot is at $p_o = 15.0$ km, and its size is $s_o = 6.0$ km. All the lengths and sizes in this spacetime are calculated proportional to the gravitational radius a.

Figure 12 is another CG example of rendering the *x*-*y* equatorial mesh lines. Note that the lines near the black hole are slightly red-shifted due to the gravitational potential. **Figure 13** is an enlarged part of a CG image example in the extreme case that the shader's output buffer is overflown. When the view point is almost in contact with the *x*-*y* equatorial plane under the similar situation to Fig. 12, the geometry shader generates too many lines beyond the output buffer's limit because the light rays bend so strongly. Each disconnected line in Fig. 13 is the corresponding evidence. Resolving the overflow in such an extreme case is our next future work (see Section 5).

4.3 Rendering Triangular Polygons

Polygon rendering has essentially the same problem as line rendering; a triangle defined by three straight lines in the black hole spacetime is not projected to a triangle defined by straight

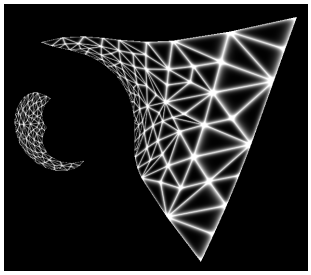

Fig. 14 CG Example of a recursively subdivided (tessellated) triangular polygon near a black hole. The horizontal angle of view is 30°. The view point is at $v = 50a$, the center of the polygon is at $p_o = 200a$, and its size s_o is $200a$.

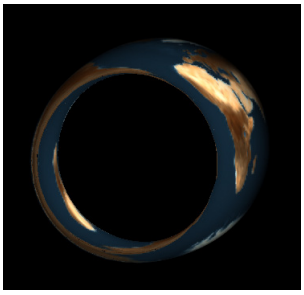

Fig. 15 CG image of the earth rotating a black hole. The horizontal angle of view is 17°. The view point is at $v = 30a$, the center of the earth is at $p_o = 20a$, and its radius s_o is $5a$.

lines but by curved lines in general. Thus we apply the recursive triangle subdivision method naturally extended from the line subdivision method in the previous subsection. This method for polygons is often called a *tessellation*. At the initial step, we project the three vertices P_1, P_2, and P_3 of a given triangle to the points S_1, S_2, and S_3 on the perspective screen, respectively, and check exactly the same terminating condition in Fig. 10 for each of the three lines S_1S_2, S_2S_3, and S_3S_1. If all the three conditions hold, we rasterize the triangle $S_1S_2S_3$ without subdivision. Otherwise we subdivide the triangle to smaller triangles recursively, where we adopt the algorithm in Ref. [18] as the concrete subdivision algorithm. For example, **Fig. 14** is the CG image of the actual rendering result of one triangular polygon. To show the triangles clearly, only their boundaries are painted with white color. The right bigger triangular mesh and the left smaller triangular mesh are rendered with the primary and secondary light rays, respectively. We see that the triangles nearer the black hole are smaller because the light rays bend stronger so that the recursion proceeds more deeply.

Three more CG examples are given in **Fig. 15**, **Fig. 16**, and **Fig. 17**. When rendering these images, the length L of every light trajectory mentioned in Section 3.4 is used for hidden surface removal. The so-called Z value cannot be used because some light rays move around the black hole more than 180°. Figure 15 is the CG image when the earth goes around the black hole. The earth is constructed from ten thousand triangular polygons onto which the texture image of the earth is mapped. We can see the similar CG image of a sphere, which is not defined by polygons, in the research paper [8]. The right hand side image of Fig. 16 is the CG image when a US space shuttle goes around the black hole, where the original modeling data [25] is shown in the left hand side. To the author's best knowledge, no existing research

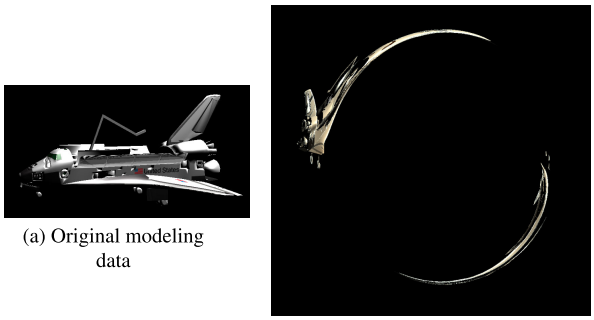

(a) Original modeling data

(b) Rendered image

Fig. 16 CG images of a US space shuttle rotating a black hole. The horizontal angle of view is 38°. The view point is at $v = 10a$, the center of the polygon is at $p_o = 5a$, and its size s_o is $2a$.

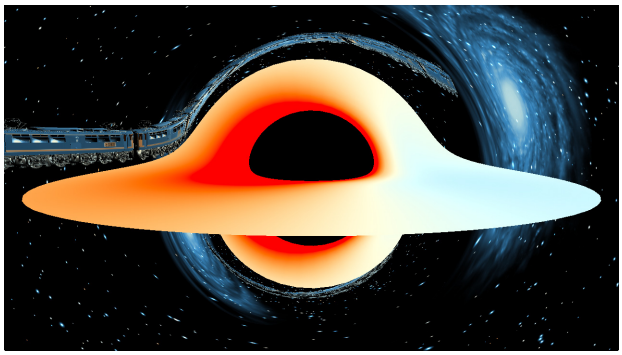

Fig. 17 CG image of a star field, a spiral galaxy, an accretion disk, and a space train of nine cars near a black hole. The horizontal angle of view is 60°. The view point is at $v = 10a$, the center of the train is at $p_o = 5a$, its length is $18a$, and its width is $0.2a$.

has ever rendered such a complex shape of CG object (modeling data) constructed with more than ten thousand polygons in a curved spacetime. The last CG example given in Fig. 17 is the combined image of the following four CG objects.

(1) A star field is rendered in the same way as in Fig. 8 as the background image.

(2) A spiral galaxy texture image [*10] mapped onto polygons is rendered as the background image.

(3) An accretion disk [3], [27] is an astronomical disk structure formed by circumstellar dust that rotates spirally around the black hole. Because the disk is rotating fast in semi-light speed [*11], the apparent color [*12] of the disk changes reddish or bluish due to the Doppler shift. The similar CG image can be seen in many research papers (e.g., Ref. [13]).

(4) A space train [*13] of nine cars is rendered, where the original modeling data [25] is the Japanese train named Sakura.

4.4 Rendering Performance

Table 3 summarizes the performances of frames per second (fps) and primitives per second (pps) for ten kinds of CG scenes

[*10] The original galaxy texture is an illustration by Mr. Shigemi Numazawa [26].

[*11] Rendering fast moving CG objects violates our assumption (recall Section 2.2). However our CG program can render it accurately with a small program modification because the disk structure is invariant to time shift even though it moves fast.

[*12] The color of the disk is calculated according to the theory of accretion disk [3] under some assumptions.

[*13] The author pays homage to the Japanese manga "*Galaxy express 999*" written and drawn by Mr. Leiji Matsumoto.

Table 3 Average frames per second (fps) and primitives per second (pps) of CG image generation.

Scene #	Primitives	CG image (Fig. #)	# objects	PC1 fps	PC1 Mpps	PC2 fps	PC2 Mpps
1	Point sprites	Star field (Fig. 8)	9,110	456.0	4.15	221.2	2.02
2	Lines	Utah teapot (Fig. 11)	928	217.5	0.20	98.5	0.09
3		X-y lattice lines (Fig. 12)	1,300	135.3	0.18	44.0	0.06
4	Polygons	Utah teapot (no ref. image)	3,136	130.6	0.41	133.1	0.42
5		Earth (Fig. 15)	9,800	83.9	0.82	64.7	0.63
6		Galaxy (part of Fig. 17)	20,000	61.0	1.22	43.0	0.86
7		Accretion disk (part of Fig. 17)	23,200	51.8	1.20	29.2	0.68
8		Space shuttle (Fig. 16 (b))	27,096	13.5	0.37	31.0	0.84
9		Space Train (part of Fig. 17)	429,876	2.6	1.12	2.1	0.90
10	Points sprites and polygons	Star field, galaxy, accretion disk, and space train (Fig. 17)	482,186	2.3	1.11	2.0	0.96

PC1: Mac Pro (Mid 2012) with ATI Radeon HD 5770
PC2: MacBook Pro (Mid 2014) with NVIDIA GT 750M

rendered on two kinds of computers, PC1 and PC2. PC1 is a slightly outdated Desktop PC, Mac Pro (Mid 2012, OS X 10.10) with ATI Radeon HD 5770, and PC2 is a high-end notebook PC, MacBook Pro (Mid 2014, OS X 10.10) with NVIDIA GT 750M. The size of all the CG images is 1,280×720 pixels [*14]. Each of the experimental results given in the table is the average value when the view point moves slowly around the black hole, watching the direction of the black hole. The host program on CPU and the shader programs on GPU are written in OpenGL/GLSL.

We observe the following from the table.

Several pps values are beyond one million pps in PC1 and near one million pps in PC2, especially for the scenes with more than ten thousand primitives. The rendering performance of point sprites is considerably higher than those of lines and polygons because the primitive subdivision is not necessary for point sprites. In other words, the subdivision process is a serious bottleneck in the whole rendering process for lines and polygons. The pps values are almost proportional to the number of CG primitives for Scenes No. 2 to 7 in Table 3, because the rendering pipeline of the GPU is accelerated by the number of primitives. The rendering performance of Scene No. 8 on PC1 is extraordinary lower than the other cases; the reason is not understood yet. The reason why the rendering performances of PC1 and PC2 are not so different is understandable from several GPU benchmarks (e.g., Ref. [28]).

5. Conclusion and Future Work

In this paper we have developed the rasterization framework for the 3D CG in a spherically symmetric black hole spacetime based on Einstein's theory of general relativity. The rasterization in this curved spacetime needs two key techniques. One is the trilinear interpolation for fast perspective projection and the other is the recursive subdivision of CG primitives for accurate rendering. As the result, we have achieved polygon rendering rates of about one million pps.

The following problems still remain on this research.

It is known that the recursive subdivision (tessellation) on the geometry shader is problematic from the view point of execution speed and GPU buffer overflow [19]. As mentioned in Section 4.4, the main reason of the slow rendering performance of lines and polygons is due to bottleneck of the tessellation. Hence our next work is to implement it with the tessellation specific shaders (the tessellation control shader and tessellation evaluation shader in OpenGL/GLSL [15], [21], [29] and the hull shader and domain shader in DirectX 11 [16]).

This paper assumes that any object stands at rest or moves slowly enough. However, the strong gravity attracts the object if it does not have an extremely powerful thruster. When the motion speed of the attracted object reaches near to light speed, the Doppler shift of light and other relativistic effects may be observed. In this sense the CG images shown in this paper include fakes. The basic treatment of relativistically fast moving objects in ray tracing is given in [8]. We must develop its extended technique in rasterization, mainly extending the boundary value problem (BVP) and its solver. Let $(t'(\tau), r'(\tau), \theta'(\tau), \phi'(\tau))$ be a four-dimensional trajectory of a polygon point with an arbitrary parameter τ, where the trajectory of an object that moves freely under the influence of gravity is defined by the geodesic equation according to the theory of general relativity. Alternatively, the trajectory of an object that has a rocket thruster may be defined programmably, in which case we should precheck if the speed of the object is below the light speed, by calculating the magnitude of the line element ds along the programmed trajectory. The extended BVP must obtain the light ray trajectory $(t(\lambda), r(\lambda), \theta(\lambda), \phi(\lambda))$ such that the light ray crosses the view point at a certain time $t(\lambda_0)$ and satisfies the equations $t'(\tau) = t(\lambda_1)$, $r'(\tau) = r(\lambda_1)$, $\theta'(\tau) = \theta(\lambda_1)$, and $\phi'(\tau) = \phi(\lambda_1)$ with $\lambda_0 > \lambda_1$. Here the technical problem is how to effectively solve it. The same tessellation techniques as in Section 4 are expected to be applicable to the solutions of this extended BVP.

The rendering performance of tablet computers is rapidly increasing. Table 3 shows that even a notebook PC can make CG images in realtime when the number of rendered polygons is not so excessive (not beyond ten thousand in the case of PC2). We expect that our research in this paper can be ported to tablet computers and run smoothly in realtime. It will have a large impact on education and entertainment.

[*14] The CG images in Fig. 11, Fig. 14, Fig. 15, and Fig. 16 are trimmed from the originally rendered images of resolution $1{,}280 \times 720$.

References

[1] Synge, J.: *Relativity: The General Theory*, North-Holland Pub. Co., Interscience Publishers, Amsterdam, New York (1960).
[2] Taylor, E.F. and Wheeler, J.A.: *Exploring Black Holes: Introduction*

to General Relativity, Addison Wesley Longman (2000).
[3] Kato, S., Fukue, J. and Mineshige, S.: *Black-Hole Accretion Disks*, Kyoto University Press (1998).
[4] Psaltis, D. and Johannsen, T.: A Ray-tracing Algorithm for Spinning Compact Object Spacetimes with Arbitrary Quadrupole Moments. I. Quasi-Kerr Black Holes, *The Astrophysical Journal*, Vol.745, No.1, p.1 (2012) (online), available from ⟨http://stacks.iop.org/0004-637X/745/i=1/a=1⟩.
[5] Nemiroff, R.: Virtual Trips to Black Holes and Neutron Stars, Michigan Technological University (online), available from ⟨http://apod.nasa.gov/htmltest/rjn_bht.html⟩ (accessed 2015-10-06).
[6] Schnittman, J.D., Krolik, J.H. and Hawley, J.F.: Light Curves from an MHD Simulation of a Black Hole Accretion Disk, *The Astrophysical Journal*, Vol.651, No.2, p.1031 (2006) (online), available from ⟨http://stacks.iop.org/0004-637X/651/i=2/a=1031⟩.
[7] kwan Chan, C., Psaltis, D. and Özel, F.: GRay: A Massively Parallel GPU-based Code for Ray Tracing in Relativistic Spacetimes, *The Astrophysical Journal*, Vol.777, No.1, p.13 (2013) (online), available from ⟨http://stacks.iop.org/0004-637X/777/i=1/a=13⟩.
[8] Kuchelmeister, D., Müller, T., Ament, M., Wunner, G. and Weiskopf, D.: GPU-based four-dimensional general-relativistic ray tracing, *Computer Physics Communications*, Vol.183, pp.2282–2290 (online), DOI: 10.1016/j.cpc.2012.04.030 (2012).
[9] Vincent, F.H., Paumard, T., Gourgoulhon, E. and Perrin, G.: GYOTO: a new general relativistic ray-tracing code, *Classical and Quantum Gravity*, Vol.28, No.22, p.225011 (2011) (online), available from ⟨http://stacks.iop.org/0264-9381/28/i=22/a=225011⟩.
[10] Weiskopf, D., Borchers, M., Ertl, T., Falk, M., Fechtig, O., Frank, R., Grave, F., King, A., Kraus, U., Müller, T.M., Nollert, H.-P., Mendez, I.R., Ruder, H., Schafhitzel, T., Schär, S., Zahn, C. and Zatloukal, M.: Explanatory and Illustrative Visualization of Special and General Relativity, *IEEE Trans. Vis. Comput. Graph.*, Vol.12, No.4, pp.522–534 (2006).
[11] Hamilton, A.J.S.: Inside Black Holes, University of Colorado (online), available from ⟨http://jila.colorado.edu/ãjsh/insidebh/⟩ (accessed 2015-10-06).
[12] Hamilton, A.J.S. and Polhemus, G.: Stereoscopic visualization in curved spacetime: seeing deep inside a black hole, *New Journal of Physics*, Vol.12, No.12, p.123027 (2010) (online), available from ⟨http://stacks.iop.org/1367-2630/12/i=12/a=123027⟩.
[13] Müller, T. and Frauendiener, J.: Interactive visualization of a thin disc around a Schwarzschild black hole, *European Journal of Physics*, Vol.33, No.4, p.955 (2012) (online), available from ⟨http://stacks.iop.org/0143-0807/33/i=4/a=955⟩.
[14] Hehl, F.W., Puntigam, R.A. and Ruder, H. (Eds.): *Relativity and Scientific Computing: Computer Algebra, Numerics, Visualization*, Springer-Verlag New York, Inc., Secaucus, NJ, USA (1996).
[15] Shreiner, D., Sellers, G., Kessenich, J.M. and Licea-Kane, B.M.: *OpenGL Programming Guide: The Official Guide to Learning OpenGL, Version 4.3*, Addison-Wesley Professional, 8th edition (2013).
[16] Luna, F.: *Introduction to 3D Game Programming with DirectX 11*, Mercury Learning & Information (2012).
[17] Zorin, D., Schröder, P., Derose, T., Kobbelt, L., Levin, A. and Sweldens, W.: Subdivision for Modeling and Animation, *SIGGRAPH 2000 Course Notes*, ACM (2000).
[18] Chung, A.J. and Field, A.J.: A Simple Recursive Tessellator for Adaptive Surface Triangulation, *J. Graph. Tools*, Vol.5, No.3, pp.1–9 (online), DOI: 10.1080/10867651.2000.10487524 (2000).
[19] Tatarinov, A.: Instanced Tessellation in DirectX10, *Game Developers Conference* (2008) (online), available from ⟨http://developer.download.nvidia.com/presentations/2008/GDC/Inst_Tess_Compatible.pdf⟩.
[20] Kessenich, J., Baldwin, D. and Rost, R.: *The OpenGL Shading Language, Version: 4.40*, The Khronos Group Inc. (2014).
[21] Sellers, G., Wright, R.S. and Haemel, N.: *OpenGL SuperBible: Comprehensive Tutorial and Reference*, Addison-Wesley Professional, 6th edition (2013).
[22] Johnson, M.H. and Teller, E.: Intensity changes in the Doppler effect, *Proc. National Academy of Sciences*, Vol.79, p.1340 (1982).
[23] Open MPI: Open Source High Performance Computing, Open MPI project (online), available from ⟨https://www.open-mpi.org⟩ (accessed 2016-02-24).
[24] Hoffleit, D. and Warren Jr., W.: Yale Bright Star Catalog, Smithsonian Astrophysical Observatory (online), available from ⟨http://tdc-www.harvard.edu/catalogs/bsc5.html⟩ (accessed 2015-10-06).
[25] de Espona, J.M.: *500 3D Objects* (*Vol.2*), Taschen (2003).
[26] Numazawa, S.: Japan Planetarium Lab. and Numazawa's Art Work, Japan Planetarium Lab. (online), available from ⟨http://www.jplnet.com/indexe.html⟩ (accessed 2015-10-06).
[27] Page, D.N. and Thorne, K.S.: Disk-Accretion onto a Black Hole. I. Time-Averaged Structure of Accretion Disk, *Astrophys. J.*, Vol.191, pp.499–506 (online), DOI: 10.1086/152990 (1974).
[28] Videocard Benchmarks, PassMark Software (online), available from ⟨http://www.videocardbenchmark.net/⟩ (accessed 2015-10-06).
[29] Wolff, D.: *OpenGL 4.0 Shading Language Cookbook*, Packt Publishing (2011).

Yoshiyuki Yamashita was born in 1959. He received his M.E. and Dr.Eng. from University of Tsukuba in 1989 and 1992, respectively. He became a research assistant at the University of Tokyo in 1989, an associate professor at University of Tsukuba in 1992, and a professor at Saga University in 2001. His current research interests include code optimization and computer graphics. He is a member of the IPSJ.